ISIJ International, Vol. 48 (2008), No. 6, pp. 747–754

Simulation Test for Crystallization of Inclusions in Semi-killed Steels during Heat Treatment Prior to Hot Rolling

Chong ZHAO,[1] Sung-Mo JUNG,[2] Yoshiaki KASHIWAYA,[3] Henri GAYE[2] and Hae-Geon LEE[2]

1) Formerly Graduate Student, Graduate Institute of Ferrous Technology (GIFT), Pohang University of Science and Technology (POSTECH). Now at China POSCO, Beijing, China. 2) GIFT, POSTECH, Pohang 790-784, Korea.
E-mail: smjung@postech.ac.kr. 3) Graduate School of Engineering, Hokkaido University, Sapporo 060-8628 Japan.

(*Received on January 16, 2008; accepted on April 3, 2008*)

The SHTT (Single Hot Thermocouple Technique) has been used to determine the crystallization behavior of a composition of the $CaO–Al_2O_3–SiO_2$ system, representative of inclusions in semi-killed steels. XRD and SEM have been employed, respectively, to detect the crystalline phases and to analyze the morphology, quantity and properties of crystals. The same composition has also been studied by quenching the oxides in iron crucibles, a method which had been proven reliable to simulate the actual behavior of inclusions in steel samples during heat treatment prior to hot rolling. The TTT diagrams obtained by using the above two techniques are almost identical. The observed crystalline phases for this composition are gehlenite ($2CaO \cdot Al_2O_3 \cdot SiO_2$) and anorthite ($CaO \cdot Al_2O_3 \cdot 2SiO_2$). The TTT diagram from SHTT gives the nose position of gehlenite and anorthite of, respectively, 1 200 s at 1 200°C and 4 800 s at 1 300°C. Thus, the Hot Thermocouple Technique (DHTT or SHTT), already largely used to study the crystallization behavior of CC mold slags is shown to be suitable to simulate the crystallization behavior of inclusions with much higher SiO_2 contents.

KEY WORDS: slag crystallization; semi-killed steel; TTT diagram; hot thermocouple; heat treatment cycle.

1. Introduction

Significant amount of work has been undertaken in the crystallization of mold fluxes used for lubrication and heat transfer control in the continuous casting process of steel. A proper precipitation of crystalline phases in mold fluxes has been known to be helpful because a significant crystal fraction in the mold fluxes reduces mold heat fluxes and helps alleviate problems associated with longitudinal cracking.[1–3]

Fewer studies on the crystallization of oxide inclusions in semi-killed steels were carried out although the presence of crystallized phases in the inclusions can affect the forming operations as well as the physical and mechanical properties of final products.[4] For instance, ruptures of steel cord during wire drawing due to spinel crystals present in the inclusions have been reported. For these steel grades, the objective is to obtain oxide inclusions that will remain glassy and plastic during metal shaping operations and to avoid the formation of hard phases such as alumina or spinels. This is firstly done by lowering the steel contents in Al, Ca and Mg to values as low as a few ppm or fractions of ppm during secondary steelmaking operations by treatments with an acid slag. The oxide inclusions present in the as-cast product are then glassy calcium and manganese alumino-silicates. However, during holding time in reheating furnaces prior to hot rolling, some of the originally glassy oxide inclusions may crystallize and thus become harmful.

A thorough understanding of the kinetics of crystallization of these calcium and manganese alumino-silicates inclusions is necessary to determine which compositions are least harmful and to control the thermal history of the steel before hot rolling. A method based on examination of synthetic oxides contained in small iron crucibles and undergoing the same thermal cycle as steel samples in reheating furnaces has been shown to give an adequate simulation of the behavior of inclusions in steel.[5] This method is however very tedious and requires a large number of experiments before the TTT diagram for a single composition can be determined.

The possibility to use the more efficient method using SHTT (Single Hot Thermocouple Technology) or DHTT (Double Hot Thermocouple Technology), largely used for mold slags,[6] would considerably simplify the determination of TTT diagrams for relevant oxide inclusion compositions. However, this method has potential limitation in the precise control of the heat treatment cycle, especially for the very long holding times required in the present situation. For some mold slag compositions, the crystallization behavior has also been shown to depend on the composition of atmosphere, and it was not obvious that the crystallization behavior in air would properly simulate the behavior of inclusions in steel.

The aim of this study is to test the applicability of SHTT or DHTT methods to simulate the crystallization of inclusions in semi-killed steels. To that effect, we selected a single composition of the $CaO–Al_2O_3–SiO_2$ system which had

been shown to exhibit a very complex crystallization behavior[5] (multinosed TTT diagram, the first crystal to appear being anorthite or gehlenite depending on holding temperature). Since the crystallization behavior around this composition had been shown to change considerably with little variation of composition,[5] we determined, from samples issued from a single batch of well homogenized master slag, the complete TTT diagrams using both experimental techniques, SHTT and heat treatment of slag contained in sealed pure iron crucibles.

2. Experimental

2.1. The SHTT Method

Figure 1 shows the schematic of the experimental apparatus which includes the single hot thermocouple (SHTT), observation system and computer data acquisition system. The data acquisition system makes it possible to measure and control the sample temperature thought the Hot Thermocouple Driver continuously and has two channel D/A (digital–analog converter: 0–5 DC volt) interfaces that can control the hot thermocouples independently (in the case of DHTT: double hot thermocouple technique). The sample is about 3 mm in diameter; therefore, an optical microscope connected to a CCD camera was used to observe the sample behavior.[6] As the video signal does not provide any information of the experimental time and temperature, a superimpose of time and characters, which exhibits the experimental conditions was connected to the video system. The computer has an image capturing system, which allows a more detailed analysis of the crystallization phenomena, permits real time digital storage of the signal and "post mortem" analysis of the rate of crystal growth.[7]

SHTT was used to apply a heat cycle on the slag sample through the Hot thermocouple driver. The desired temperature and holding time were controlled by computer and the nucleation and crystal growth were observed through the monitor screen connected to the VCR *in situ* and *ex situ*. Furthermore, an air cooling device for attaining the rapid quenching was installed and activated by a computer signal synchronized with the turn-off of the electric power of furnace and hot thermocouple. Compressed air (1 atm and ambient temperature) was blown onto the sample *via* electromagnetic valve and the cooling rate of 400°C/s within 2 s from the starting of cooling was attained.[10]

Synthetic master slag based on the $CaO–SiO_2–Al_2O_3$ system was prepared by mixing high-purity (99.5 to 99.95%) chemicals of $CaCO_3$, SiO_2 and Al_2O_3 at an appropriate proportion. About 100 g of the oxide mixtures of desired composition were pre-melted in platinum crucibles in a box furnace (3 h at 1 500°C) and poured onto a copper plate. They were then finely crushed and melted again for enhanced homogenization. After quenching and crushing, the slag compositions were chemically analyzed. The composition of the sample used in this study is listed in **Table 1**. The melts of the synthetic slags used in this study were transparent and the precipitated crystals were clearly visible. In addition, the measurement of the number of nucleation events and the rate of crystal growth were significantly distinct with the help of the automated computer image analysis employed.

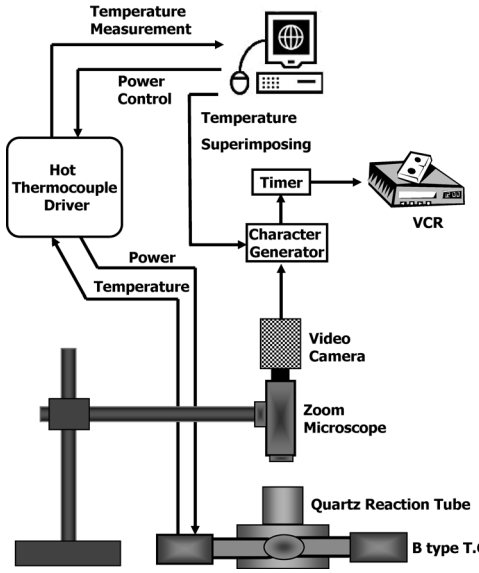

Fig. 1. Schematic diagram of the experimental apparatus for SHTT.

Table 1. Chemical composition of $CaO–Al_2O_3–SiO_2$ slag.

Oxides	CaO	Al_2O_3	SiO_2	CaO/SiO_2
mass%	35.4	25.2	39.4	0.90

2.2. Heat Treatment in Sealed Fe Crucibles

Pure iron rod (4N, [mass%C]$<$0.01) was machined to prepare iron crucibles (OD: 15 mm, height: 22 mm) to which about 5 g of finely crushed slag powders was charged. The crucibles containing slag powder were then put into a quartz tube and sealed under vacuum in order to prevent oxidation of the outside of the crucible during the heat treatment. The heat cycle procedure was carried out in a horizontal resistance furnace in Ar atmosphere. They consist of 5 min of premelting stage at the temperature of 50°C higher than the liquidus temperature of the oxide mixture, and an isothermal holding period of desired time by moving the crucible assembly in a predefined cooler zone of the furnace. The temperature was measured with a thermocouple set against the crucible wall. The measured cooling time to the isothermal plateau between 800 and 1 400°C was about 5 s per 100°C. At the end of the holding period, the crucible was rapidly withdrawn from the furnace and water quenched. This operation took 5 to 10 s. The samples were then cut, and the polished sections were observed using optical or scanning electron microscopy. The detected crystals were identified by SEM-EDS or XRD for some experiments.

3. Results and Discussion

3.1. *In-situ* Observation of Oxide Crystallization

Figure 2 shows the sequence of crystal precipitation and growth observed in the sample at 1 200°C. It could be determined from this observation that the nose time of crystallization was 1 200 s which is quite long time comparing to a mold slag[11] and a blast furnace slag.[10] Figure 2 indicated the crystal growth at 50 s, 1 250 s, 4 500 s and 6 300 s

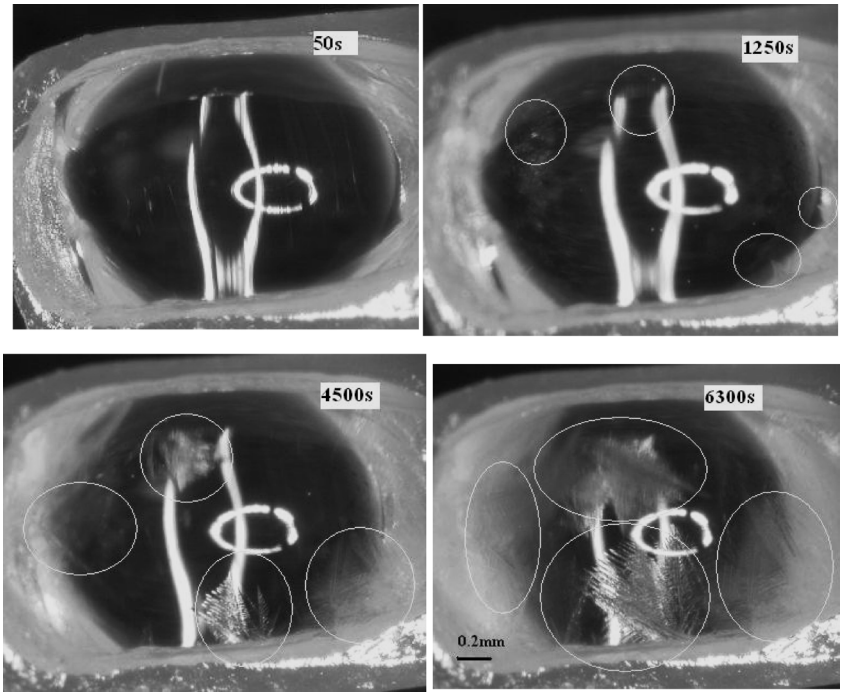

Fig. 2. Crystallization behavior of slag at 1 200°C.

from the beginning of experiments, respectively. It is also interesting that the crystal morphology was clear dendrite. The positions of crystals are noted with yellow circles and the white rings in the center of those pictures appeared due to the microscope reflection.

When the experimental temperature was decreased to 1 000°C, the sizes of crystals were very small, thus making it difficult to accurately measure the initial crystal size. To examine the morphology of the crystals, the sample was quenched to 1 000°C from 1 500°C then quenched to room temperature after crystallization had initiated. From a SEM observation, it was found that many small dendrites already existed.

3.2. Identification of Crystal Phases and Determination of TTT Diagram by XRD

XRD analysis was performed to identify the crystal phases in the obtained tentative TTT diagram of the master slag. The holding temperatures were decided to be that at the nose (1 200°C) and both sides of the temperature (1 320°C and 1 105°C). At first, the holding times were 3 000, 8 000 and 12 000 s, *etc.* at those three temperatures (1 320, 1 200 or 1 105°C). The amount of sample used was about 10 mg, which later was found to be small for a conventional XRD analysis; consequently, the measurement conditions of XRD were selected to be as high power as possible (30 kV, 300 mA, Cu-Kα). Furthermore, the scan speed was at 0.25°/min from 20 to 90 degrees in terms of 2θ angle.[8,10] From this method, the crystal phases in the sample obtained from SHTT were identified with relatively high accuracy and reproducibility.

Figure 3 shows the typical example of XRD data of this slag quenched to 1 200°C holding at 3 000, 8 000, 12 000 and 13 000 s, respectively, in which the crystallization was observed in every typical stage. The obtained peaks were complicated. From the sample composition, gehlenite

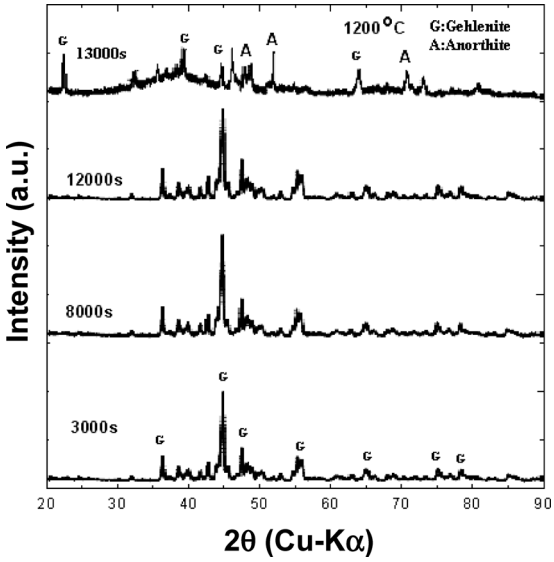

Fig. 3. Determination of crystal phase precipitation in the slag quenched to 1 200°C for 3 000 s.

(ASTM9-216: C_2AS: $2CaO \cdot Al_2O_3 \cdot SiO_2$) is the dominant phase in this system from 3 000 to 12 000 s. When the holding time proceeded onto 13 000 s, anorthite was also detected in this slag phase, which means after 13 000 s, gehlenite and anorthite coexist in this system.

Although both gehlenite and anorthite existed at 1 200°C, the amount of gehlenite increased with the increasing holding time. This tendency was similar to the results at 1 320 and 1 050°C as shown in **Figs. 4** and **5**. Figures 4 and 5 show the XRD analysis results of the samples quenched to other two different temperatures, 1 320 and 1 105°C, respectively. Figure 4 shows the XRD patterns of the sample held at 1 320°C for 3 000, 8 000 and 12 000 s. The crystal phase was identified to be anorthite ($CaO \cdot Al_2O_3 \cdot 2SiO_2$) at 1 320°C. For the holding time of

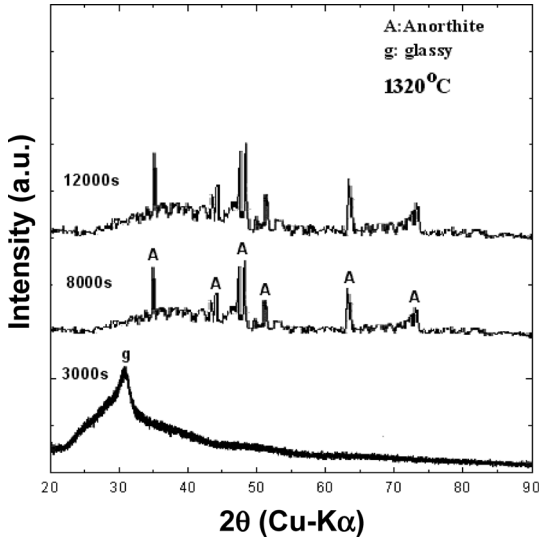

Fig. 4. Determination of crystal phase precipitation in the slag quenched to 1 320°C, then holding for 3 000 s and 12 000 s.

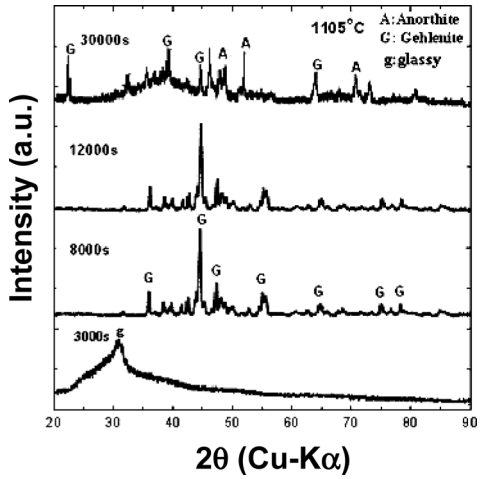

Fig. 5. Determination of crystal phase precipitation in the slag quenched to 1 105°C for 3 000 s and 30 000 s, respectively.

3 000 s, the slag still remained glassy in this case. Those peaks were not as intense and discernible as the one at the lower temperature as shown in Fig. 5. Furthermore, the data scattering was relatively large. At 1 105°C, the beginning time of crystallization was 2 800 s, and after 30 000 s, gehlenite and anorthite coexisted in the system.

To improve the two phase region in the TTT diagram, another set of XRD measurement was made on the quenched sample from 1 300°C at several holding times. **Figure 6** shows the results of XRD analysis in this condition. The incubation time of anorthite was 4 800 s at 1 300°C. From Fig. 6, it was proven that anorthite and gehlenite coexist in the system after 8 000 s at 1 300°C. **Figure 7** shows the results of XRD for identifying the crystal phases in the initial precipitation stage of crystallization at different holding temperatures.

Finally, the TTT diagram was determined as shown in **Fig. 8**. It modified the single crystal phase curve in the tentative TTT diagram obtained from *in situ* observation to the double noses TTT curves. The upper nose in the final TTT diagram obtained by XRD analysis would be the nose of

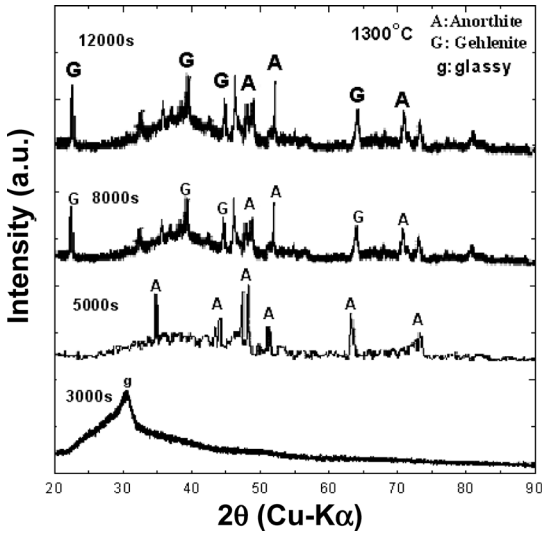

Fig. 6. Determination of crystal phase precipitation in the slag quenched to 1 300°C for 3 000 s and 12 000 s, respectively.

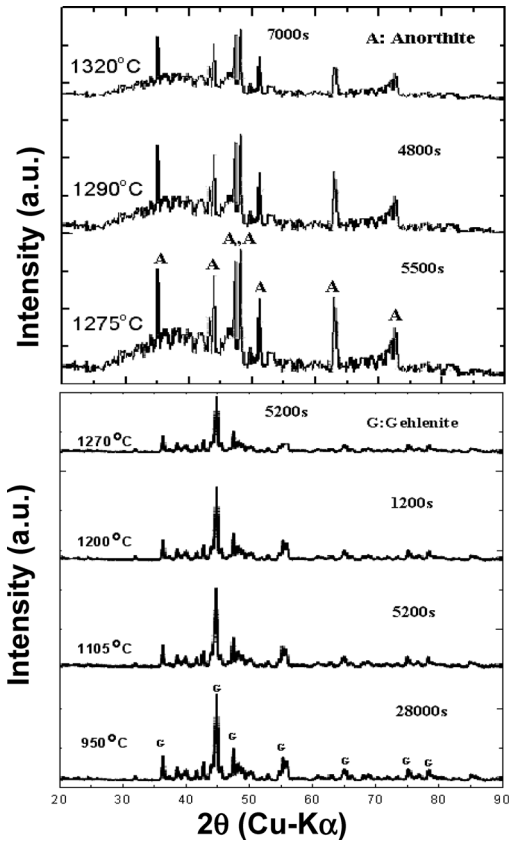

Fig. 7. XRD pattern comparison of a slag in the temperature range from 950 to 1 320°C at different holding times.

anorthite and the lower one indicated that of gehlenite. The anorthite crystals precipitated at higher temperature were transparent or translucent, which were difficult to identify by the naked eyes. The nose of anorthite was located around 4 800 s at 1 300°C and that of gehlenite was around 1 200 s at 1 200°C. The reason why gehlenite precipitates faster than anorthite can be explained in terms of free energy functions of the compounds, which will be discussed in the following part. The experimental data are listed in **Table 2**.

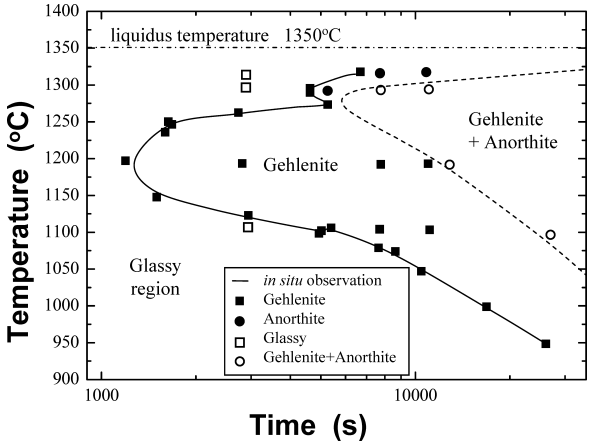

Fig. 8. TTT diagrams of the beginning of crystallization obtained by *in situ* and *ex situ* observations using optical microscope and XRD analysis.

3.3. Crystal Growth Curve in High Temperature Region

Image analyses were performed to evaluate the volume fraction of crystals evolved as a function of time. As previously mentioned, it was difficult to perform automatic image analysis since computerized edge detection was not possible. The portion of the clearly recognizable crystals was manually outlined in each frame, and their areas were evaluated by computer. Although the reproduction of the detailed crystal outline was not exact, a total of 200 000 pixels were used for calculation and the error was estimated to be within ±5% uncertainty from several calculations. The variation of crystal volume fraction with time was plotted in **Fig. 9**. It is useful to describe the incubation time from this sort of figure. The area fraction of crystals was taken by Photoshop® to compare the frame of crystals with that of the overall sample such as **Fig. 10** taken on 4 200 s at 1 200°C.

Table 2. Experimental data for SHTT.

Exp. No.	Temp(°C)	Time(sec)	Observed Phases	Fraction of Crystal (Area%)
01-SHTT	1320	3000	Glassy	None
02-SHTT	1320	7000	Anorthite	32
03-SHTT	1320	8000	Anorthite	35
04-SHTT	1320	12000	Anorthite	65
05-SHTT	1300	3000	Glassy	None
06-SHTT	1300	4800	Anorthite	30
07-SHTT	1300	5000	Anorthite	32
08-SHTT	1300	8000	Anorthite	32
			Gehlenite	66
09-SHTT	1300	12000	Anorthite	32
			Gehlenite	66
10-SHTT	1290	4800	Anorthite	40
11-SHTT	1275	5500	Anorthite	45
12-SHTT	1265	2800	Gehlenite	45
13-SHTT	1255	1650	Gehlenite	48
14-SHTT	1250	1700	Gehlenite	50
15-SHTT	1240	1600	Gehlenite	52
16-SHTT	1200	1200	Gehlenite	50
17-SHTT	1200	3000	Gehlenite	60
18-SHTT	1200	8000	Gehlenite	60
19-SHTT	1200	12000	Gehlenite	60
20-SHTT	1200	13000	Gehlenite	60
			Anorthite	45
21-SHTT	1150	1500	Gehlenite	35
22-SHTT	1125	3000	Gehlenite	38
23-SHTT	1110	5600	Gehlenite	35
24-SHTT	1105	3000	Glassy	None
25-SHTT	1105	5200	Gehlenite	40
26-SHTT	1105	8000	Gehlenite	55
27-SHTT	1105	12000	Gehlenite	60
28-SHTT	1105	30000	Gehlenite	60
			Anorthite	35
29-SHTT	1100	5100	Gehlenite	42
30-SHTT	1080	8000	Gehlenite	40
31-SHTT	1075	9000	Gehlenite	38
32-SHTT	1050	11000	Gehlenite	35
33-SHTT	1000	18000	Gehlenite	35
34-SHTT	950	28000	Gehlenite	30

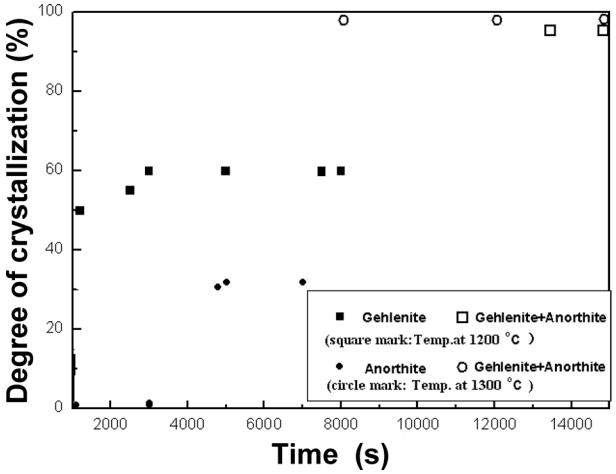

Fig. 9. Variation of crystal fraction at 1 200 and 1 300°C for this slag.

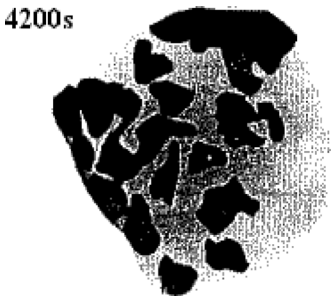

Fig. 10. Crystallized area in slag.

From Fig. 9, the first phase to crystallize is gehlenite as observed by *in situ* observation and XRD data at 1 200°C. Gehlenite crystals occupy up to the maximum 60% of the total volume as estimated by image analysis. The final 95% crystallization (gehlenite: 60%, anorthite: 30%, remaining glass: 5%) is then reached after holding the sample longer than 12 000 s at 1 200°C. While the first crystallized phase was anorthite after 8 000 s at 1 300°C, the final 98% crystallization (anorthite: 32%, gehlenite: 66%, remaining glass: 2%) was performed. Nucleation and growth mechanisms of crystals are not of a primary concern in this study. Therefore, the crystallization-induced volume change was calculated only by image analysis, which was not precise. The further quantitative analysis by XRD will be preformed in the future.

3.4. Driving Force for Crystallization

According to the thermodynamic theory, the driving force for crystal precipitation is volume-free energy change (standardized at 1 gram-atom) for the crystallization of an infinitesimal amount of the phase at the expense of the meta-stable liquid phase.[4] The activities of the compounds in the slag were estimated by FACTSAGE® at a series of temperatures. The standard free energy change for the precipitated crystals (Gehlenite and Anorthite) was plotted as a function of temperature in **Fig. 11**.[9] The two curves represented by the free energy change of anorthite (CAS_2) and gehlenite (C_2AS) intersect with each other at around 1 180°C, which is slightly different from the boundary temperature in the TTT diagrams. The difference may be caused by the database chosen in FACTSAGE®. Furthermore, the interfacial energy of the precipitated crystal was not taken into account in the current calculation due to the lack of the interfacial energy data. In addition, a term of kinetics such as a diffusion of elements for the crystallization should be included in the result of TTT diagram.

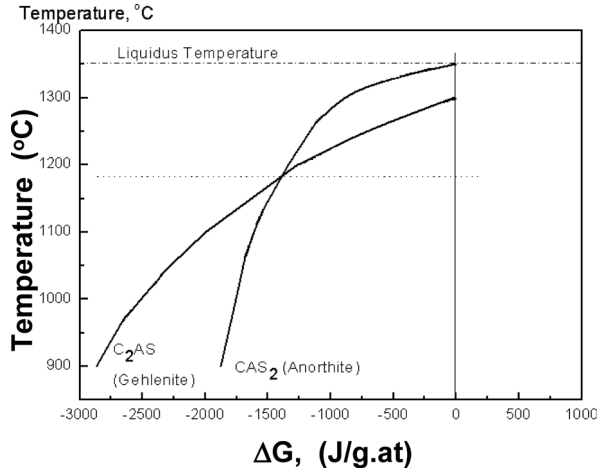

Fig. 11. Evaluation of the volume-free energy change for the formation of the various solids from the supersaturated liquid.

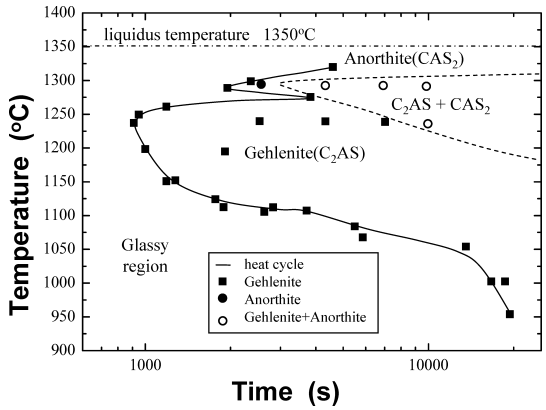

Fig. 12. TTT diagrams displaying the crystallization start conditions obtained by heat cycle experiment.

However, Fig. 11 indicates that anorthite is more stable than gehlenite above 1 180°C, which explains that anorthite (CAS_2) first precipitated. This was also predicted from the TTT diagrams. On the other hand, gehlenite (C_2AS) is more stable than anorthite below 1 180°C. Accordingly, gehlenite precipitated earlier than anorthite.

3.5. Comparison of SHTT Results with Those from Heat Treatment Cycle by Using Iron Crucible

As previously mentioned, the heat treatment by HTT cannot be sophisticatedly controlled since the sample is exposed to external atmosphere directly. Accordingly, a closed system was required to perform an accurate and precise heat treatment cycle. **Figure 12** shows the final TTT diagram from heat treatment cycle which clearly contributed to two different crystal phases and the coexisting region. The dominant crystals evolved in this slag were also gehlenite and anorthite. The incubation time for gehlenite was 900 s at 1 240°C and that for anorthite was 2 000 s at 1 290°C which were shorter time than the result of Hot thermocouple method. For the sake of reference, a series of

Table 3. Experimental data for heat treatment cycle.

Exp. No.	Temp(°C)	Time(sec)	Observed Phases	Fraction of Crystal (Area%)
01-HT	1320	5000	Anorthite	32
02-HT	1300	2500	Anorthite	35
03-HT	1290	2000	Anorthite	38
04-HT	1290	3000	Anorthite	40
05-HT	1290	5000	Anorthite	40
			Gehlenite	52
06-HT	1290	8000	Anorthite	40
			Gehlenite	52
07-HT	1290	12000	Anorthite	40
			Gehlenite	52
08-HT	1275	4100	Gehlenite	42
09-HT	1265	1200	Gehlenite	45
10-HT	1250	950	Gehlenite	45
11-HT	1240	900	Gehlenite	50
12-HT	1240	3000	Gehlenite	55
13-HT	1240	5000	Gehlenite	55
14-HT	1240	8000	Gehlenite	55
15-HT	1240	12000	Gehlenite	55
			Anorthite	40
16-HT	1200	1000	Gehlenite	48
17-HT	1150	1200	Gehlenite	45
18-HT	1150	1400	Gehlenite	42
19-HT	1125	1800	Gehlenite	40
20-HT	1123	2000	Gehlenite	40
21-HT	1110	4000	Gehlenite	47
22-HT	1110	4200	Gehlenite	45
23-HT	1105	2800	Gehlenite	42
24-HT	1080	6000	Gehlenite	45
25-HT	1070	6300	Gehlenite	43
26-HT	1050	15000	Gehlenite	45
27-HT	1000	19000	Gehlenite	35
28-HT	1000	20000	Gehlenite	37
29-HT	950	22000	Gehlenite	32

experimental data were listed in **Table 3**.

These obtained two TTT diagrams are compared in **Fig. 13**. Each of the curves in the TTT diagrams showed the similar double C shape. The difference of incubation time from the previous *in-situ* observation experiment might be due to the slight temperature difference of SHTT between the junction point of the thermocouple and sample position to be crystallized. The two TTT curves are in approximately good agreement with each other. This indicated that SHTT can be an appropriate experimental method dealing with slag heat treatment, and it typically gave good coincidence with the classical heat treatment cycle for the slag compositions investigated. For other slag compositions, the coincidence between HTT technique and heat treatment cycle should be further investigated. From the results obtained in this study, it is obvious that the main advantage of DHTT or SHTT is to directly observe the crystallization phenomena related to non-metallic inclusions.

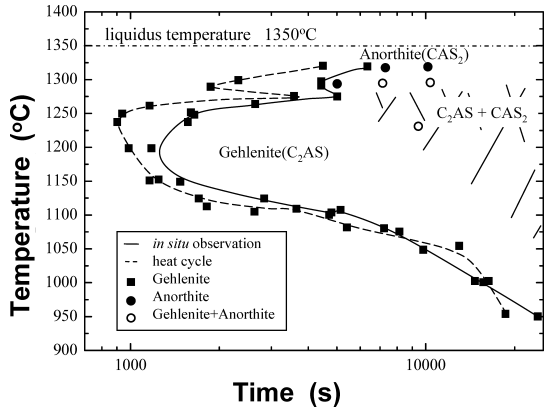

Fig. 13. Comparison of TTT diagrams resulted from *in-situ* observation and heat cycle experiment.

4. Conclusions

The crystallization behavior of a composition of the $CaO–Al_2O_3–SiO_2$ slag system was investigated by obtaining TTT diagrams using SHTT (Single Hot Thermocouple Technique) and heat treatment cycle analysis. The similarity of the TTT curves obtained from the two methods confirms that the much faster and easier SHTT method is appropriate to simulate the crystallization behavior of glassy inclusions in semi-killed steels.

The following results were obtained:

(1) The liquidus temperature of the master slag used in the present study was 1 350°C.

(2) Crystal phases in the TTT diagram for this slag were identified to be gehlenite ($2CaO \cdot Al_2O_3 \cdot SiO_2$) and anorthite ($CaO \cdot Al_2O_3 \cdot 2SiO_2$).

(3) Anorthite crystals appear first at higher temperature, and gehlenite at lower temperature. The nose position of gehlenite in the obtained TTT diagrams was 1 200 s at 1 200°C from SHTT and 900 s at 1 240°C from heat cycle experiment. The nose of anorthite was 4 800 s at 1 300°C from SHTT and 2 000 s at 1 290°C from heat cycle experiment.

(4) The variations of crystal fractions with holding time for the two methods were also in good agreement.

(5) The volume-free energy change data for the formation of the various crystals were evaluated to interpret the crystallization phenomena occurring in the TTT diagrams from the standpoint of thermodynamic theory.

REFERENCES

1) P. V. Riboud and M. Larrecq: Proc. of 62nd Steelmaking Conf., ISS, Warrendale, PA, (1979), 78.
2) K. Mills, M. Susa and V. Ludlow: Proc. of 14th Process Technology Conf., ISS, Warrendale, PA, (1995), 157.
3) A. Yamaguch, K. Sorimachi, T. Sakuraya and T. Fuji: *ISIJ Int.*, **33** (1993), 140.
4) P. V. Riboud, C. Gatellier, H. Gaye, J. N. Pontoire and P. Rocabois: *ISIJ Int.*, **36** (1996), S22–S25.
5) P. Rocabois, J. N. Pontoire, J. Lehmann and H. Gaye: *J. Non-Cryst. Solids*, **282** (2001), 98.
6) Y. Kashiwaya, C. E. Cicutti, A. W. Cramb and K. Ishii: *ISIJ Int.*, **38** (1998), No. 4, 348.
7) C. Orrling, S. Sridhar and A. W. Cramb: *ISIJ Int.*, **40** (2000), No. 9, 877.
8) C. Tse, S. H. Lee, S. Sridhar and A. W. Cramb: Proc. of 83rd Steelmaking Conf., ISS, Warrendale, PA, (2000), 219.
9) I. Brain: Thermochemical Data of Pure Substances, VCH, New York, (1989), 311, 312.
10) Y. Kashiwaya, T. Nakauchi, K. S. Pham, S. Akiyama and K. Ishii: *ISIJ Int.*, **47** (2007), 44.
11) Y. Kashiwaya, C. E. Cicutti and A. W. Cramb: *ISIJ Int.*, **38** (1998), 357.